



This is a repository copy of *Experimental and analytical investigation of a new three-dimensional seismic isolation under coupled horizontal-vertical excitations*.

White Rose Research Online URL for this paper:

<https://eprints.whiterose.ac.uk/226171/>

Version: Published Version

Article:

Pourmasoud, M., Hajirasouliha, I. orcid.org/0000-0003-2597-8200, Lim, J.B.P. et al. (1 more author) (2025) Experimental and analytical investigation of a new three-dimensional seismic isolation under coupled horizontal-vertical excitations. *Journal of Earthquake Engineering*. ISSN 1363-2469

<https://doi.org/10.1080/13632469.2025.2484602>

Reuse

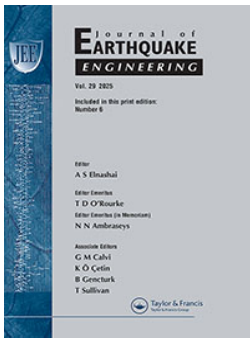
This article is distributed under the terms of the Creative Commons Attribution-NonCommercial-NoDerivs (CC BY-NC-ND) licence. This licence only allows you to download this work and share it with others as long as you credit the authors, but you can't change the article in any way or use it commercially. More information and the full terms of the licence here: <https://creativecommons.org/licenses/>

Takedown

If you consider content in White Rose Research Online to be in breach of UK law, please notify us by emailing eprints@whiterose.ac.uk including the URL of the record and the reason for the withdrawal request.



eprints@whiterose.ac.uk
<https://eprints.whiterose.ac.uk/>



Experimental and Analytical Investigation of a New Three-Dimensional Seismic Isolation Under Coupled Horizontal-Vertical Excitations

Masoud Pourmasoud, Iman Hajirasouliha, James B.P Lim & Amirmahmoud Behzadi

To cite this article: Masoud Pourmasoud, Iman Hajirasouliha, James B.P Lim & Amirmahmoud Behzadi (07 Apr 2025): Experimental and Analytical Investigation of a New Three-Dimensional Seismic Isolation Under Coupled Horizontal-Vertical Excitations, Journal of Earthquake Engineering, DOI: [10.1080/13632469.2025.2484602](https://doi.org/10.1080/13632469.2025.2484602)

To link to this article: <https://doi.org/10.1080/13632469.2025.2484602>



© 2025 The Author(s). Published with license by Taylor & Francis Group, LLC.



Published online: 07 Apr 2025.



Submit your article to this journal [↗](#)



Article views: 158



View related articles [↗](#)



View Crossmark data [↗](#)

Experimental and Analytical Investigation of a New Three-Dimensional Seismic Isolation Under Coupled Horizontal-Vertical Excitations

Masoud Pourmasoud^a, Iman Hajirasouliha ^b, James B.P Lim^c, and Amirmahmoud Behzadi^d

^aDepartment of Civil and Environmental Engineering, University of Auckland, Auckland, New Zealand; ^bDepartment of Civil and Structural Engineering, The University of Sheffield, Sheffield, UK; ^cSchool of Engineering, The University of Waikato, Hamilton, New Zealand; ^dDepartment of European and Mediterranean Cultures, Environment, and Cultural Heritage, University of Basilicata, Potenza, Italy

ABSTRACT

This study investigates experimentally and analytically the performance of a new Three-Dimensional Seismic Isolator (3DSI) designed to control the horizontal-vertical coupled responses of multi-story buildings. The proposed isolator system adopts the concept of Super-High-Damping-Rubber (SHDR) to achieve vertical isolation by decreasing the vertical effective stiffness and increasing the vertical effective damping, thus minimizing the imparted vertical acceleration into the superstructure. Three different case-study buildings, including dual 5-story steel frames with Fixed Base, Conventional Seismic Isolators (CSI), and the proposed 3DSI, were analysed using OpenSees software based on experimentally validated models under a set of 12 earthquake records. The vertical period of the isolator system was tuned to reach 0.3 s, at which most of the vertical ground motions are degraded to less than 2.0 g. The results indicate that the proposed 3DSI system can considerably decrease the vertical and horizontal responses by up to 65% and 20%, respectively, compared to the CSI system. It is shown that using the 3DSI system minimizes the potential damage by reducing the magnitude of the vertical responses, while it also leads to smaller compression and tension axial loads and less inter-story drifts. In contrast, Fixed Base and CSI buildings experienced significantly escalated vertical accelerations, particularly on long-span beams, potentially leading to extensive non-structural damage during strong earthquake events.

ARTICLE HISTORY

Received 30 October 2024
Accepted 20 February 2025

KEYWORDS

Conventional seismic isolation; three-dimensional seismic isolation; vertical acceleration; coupled horizontal-vertical excitation; damage level; SHDR layers

1. Introduction

The performance of structural elements depends significantly on inter-story drift, while non-structural elements are more sensitive to acceleration. For essential buildings such as hospitals, over 90% of the project cost is allocated to non-structural elements and contents (FEMA E-74 2012). The coupling of horizontal-vertical excitations might cause medium to complete damage to non-structural elements (Cancellara and De Angelis 2016; Pourmasoud et al. 2020). Although Conventional Seismic Isolators (CSI) are effective in reducing floor accelerations, they are not generally suitable for mitigating vertical responses in structures (Dong et al. 2023; Guzman, Jean, and Ryan 2018; M. Kumar, Whittaker, and Constantinou 2014). In a typical building, the objects start to shake when vertical acceleration exceeds 1.0 g and damage happens when it goes beyond 2.0 g (Furukawa et al. 2013). Experimental test results show that vertical accelerations

CONTACT Masoud Pourmasoud  mpou570@aucklanduni.ac.nz  Department of Civil and Environmental Engineering, University of Auckland, 1 Leander Place, Flagstaff, Hamilton, New Zealand

© 2025 The Author(s). Published with license by Taylor & Francis Group, LLC.

This is an Open Access article distributed under the terms of the Creative Commons Attribution-NonCommercial-NoDerivatives License (<http://creativecommons.org/licenses/by-nc-nd/4.0/>), which permits non-commercial re-use, distribution, and reproduction in any medium, provided the original work is properly cited, and is not altered, transformed, or built upon in any way. The terms on which this article has been published allow the posting of the Accepted Manuscript in a repository by the author(s) or with their consent.

between 2.0 and 5.0 g can cause moderate to extensive damage, and buildings with higher vertical accelerations may suffer complete non-structural damage (Ryan et al. 2016; Soroushian et al. 2016).

Following the Christchurch earthquake, vertical PGAs of up to 2.18 g were recorded at the HVPS station. The vertical PGA can amplify along the height of seismic isolated multi-story buildings, posing significant structural and non-structural challenge that can impact building functionality. Moreover, vertical excitations can amplify horizontal responses, necessitating increased lateral displacement capacity. Therefore, seismic isolation designers must account for the coupled effects of horizontal and vertical excitations on seismically isolated buildings, rather than focusing solely on horizontal effects.

In recent years, there has been a growing interest in the development of three-dimensional seismic isolators, as building in near field zones with high vertical peak ground acceleration (PGA) is unavoidable in many regions. For example, Wellington (New Zealand), California (USA), and Jakarta (Indonesia) are among the cities where buildings and infrastructure have extended in the vicinity of active faults. Therefore, to reduce the risk of near field earthquakes with high vertical accelerations, it has been suggested to replace Conventional Seismic Isolators (CSIs) with more efficient seismic isolation systems such as Three Dimensional Seismic Isolators (3DSIs) to effectively mitigate both horizontal and vertical ground motions (Pourmasoud et al. 2020).

As one of the first attempts, Fujita et al. (1996) conducted a feasibility study to develop 3DSIs by adopting rubber isolators in the horizontal direction and coned-disc springs for vertical isolation, with a target frequency of 3 Hz. They vertically stacked several rubber isolators by connecting the load plates and having the spring on top to decrease the vertical stiffness and achieve the desired frequency. While this methodology was relatively successful, it was not considered practical or financially viable for typical buildings. Similar investigations were conducted by Morishita, Inoue, and Fujita (2004), Koo et al. (2022) and Yu et al. (2023) which confirmed the good performance of such systems in controlling the vertical vibrations.

In another relevant study, Yabana and Matsuda (2000) proposed using thick rubber layers and a low shape factor (approximately 4.0) to achieve a 0.3 Hz frequency in the vertical direction and decrease seismic actions. It should be noted that the shape factor for Conventional Seismic Isolators (CSIs) is typically greater than 15 to prevent the isolator from buckling under high axial loads and large lateral displacements (Skinner, Robinson, and McVerry 1993). However, using the thick rubber layer concept can reduce the load capacity of isolators.

The use of hydraulic systems with rubber bearings and high-pressure air springs has been investigated by several researchers, including Inoue et al. (2004) and Suhara et al. (2005) who suggested that an ideal three-dimensional isolator should have a frequency range of 0.5–0.67 Hz and a damping ratio higher than 5%. Additionally, Zhou, Wong, and Mahin (2016) studied the seismic responses of a 3DSI nuclear power plant and concluded that isolators with a vertical frequency less than 3.0 Hz could effectively reduce vertical responses.

To develop a three-dimensional seismic isolation with low vertical stiffness, combination of laminated lead rubber bearing and a ring spring were experimentally investigated by Liang et al. (2022). In 2024, Mo et al. introduced an air spring – lead rubber bearing (AS-LRB) seismic isolation device to improve the performance of lightweight flexible structures. Similarly, Luo et al. (2024) proposed a combination of improved laminated natural rubber bearings and spring bearings to increase seismic resiliency in buildings subjected to metro and earthquake vibrations. Another similar system consisting of thick rubber bearing (TNRB), disc spring bearing (DSB), and laminated rubber bearing (LRB) was designed by Gu et al. (2024). Increasing the vertical damping of elastomeric isolators by utilizing viscoelastic damping technology was investigated by Hu et al. (2024).

Shi et al. (2023), proposed a separated three-dimensional isolation scheme, placing horizontal isolators at the base of the superstructure and vertical isolators under floor slabs, to improve seismic performance. In addition, to provide vertical isolation for the friction pendulum sliders, Cao et al. (2023) tested a combination of thick laminated rubber bearings and a friction pendulum (3D-VIB).

The Negative Stiffness Devices (NSD) concept, originally introduced by Sarlis et al. (2013) involves weakening the structural system and adding damping without causing permanent deformation to reduce seismic responses. In a relevant study, Cimellaro, Domaneschi, and Warn (2018) suggested the use of NSD in the vertical direction to achieve smaller vertical accelerations than conventional isolation methods. More recently, in 2023, He et al. (2023) introduced a 3D isolation system with high-static-low-dynamic stiffness (HSLDS), featuring a negative stiffness device and a pre-deformed inclined rubber bearing. In the same year, Xu et al. (2023) conducted a shaking table test to evaluate the seismic performance of a three-dimensional seismic isolation system featuring inclined rubber bearings.

In another study, Pourmasoud et al. (2020) designed the concept of a three-dimensional seismic isolation system (3DSI) with the objective of developing a system that could increase the vertical effective damping and decrease the vertical responses while maintaining all the horizontal specifications of an elastomer bearing. To achieve this, a Super High Damping Rubber (SHDR) layer, which is horizontally restrained against lateral movements, was added on top of a Lead Rubber Bearing (LRB) to provide vertical stiffness and damping. This enabled the vertical specifications to be adjustable without impacting the horizontal specifications.

The primary advantage of the proposed 3DSI is its capability to independently adjust the vertical and horizontal characteristics (effective stiffness and damping) based on the seismic demands (vertical and horizontal PGAs) of a given region. This feature is particularly beneficial for near-fault zones, such as Wellington City, New Zealand, where high vertical accelerations are expected. The design ensures that the rubber properties in the horizontal and vertical directions are specifically optimized for their respective performance requirements.

In the horizontal direction, the rubber must accommodate large displacements, often reaching several hundred millimeters, necessitating a high shear strain capacity. To meet this demand, natural rubber with low damping and high elongation properties was used. Conversely, the vertical direction requires rubbers with high damping capacity to manage small deformations, typically less than 50 mm. To achieve this, additives were introduced into the SHDR layers. While these additives reduce deformation capacity, they significantly enhance damping, making the system more effective in handling vertical seismic forces.

Figure 1 depicts the proposed 3DSI before and after lateral displacement. The total vertical stiffness of the proposed 3DSI comprises the vertical stiffness of the LRB at a certain lateral displacement, as well as the vertical stiffness of the SHDR layers.

It is worth noting that although high damping rubber layers provide reasonably higher effective damping (6% to 12%) compared to natural rubber layers (<5%), they have limited shear strain capacity, making them less ideal for large displacements. In this concept, the rubber layer specifications are adjusted to ensure their appropriate utilization of their capacity. Specifically, the SHDR layer

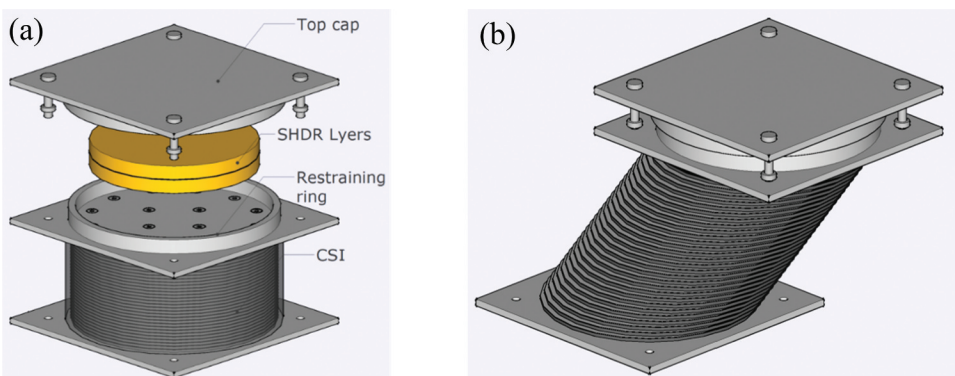


Figure 1. Proposed 3DSI with SHDR layer: a) undeformed, b) deformed.

is designed to cope with restricted deformations from vertical excitation and provide high vertical effective damping, while the natural rubbers are intended to handle large lateral displacements. The number and thickness of SHDR layers are determined based on the required vertical stiffness and rubber shear strain under axial loads.

2. Numerical Study

2.1. Superstructure

To demonstrate the efficiency of the proposed 3DSI with SHDR in practical applications, a five-story building was considered as a case study example. The structure was modelled using the OpenSees software (McKenna, Scott, and Fenves 2000), as a dual system consisting of intermediate steel moment frames and braces. The floor height is 4 m, while each frame has three spans of 6.0 m, 6.0 m, and 9.0 m to investigate the influence of vertical acceleration on medium to long spans. The structural elements were designed based on the requirements of a high seismic zone, as specified in the 2022. Figure 2 shows the 2D fixed base building model developed in OpenSees. The columns were modelled as hollow section boxes sized 430×430 mm and 400×400 mm, with St52 steel plates of 30 mm thickness. The beams were built up elements using I sections with heights of 450 mm and 600 mm, forming spans of 6 m and 9 m, respectively. The beam wings were 250 mm \times 25 mm using St37 steel plates. The bracing elements were modelled as 100 mm hollow section boxes. The applied dead load, live load, and partition loads were assumed as 2.80, 2.50, and 0.5 kN/m² in addition to the structure self-weight.

To account for the potential plastic behaviour of the column and beam elements under seismic loads, the force-based beam-column element and displacement-based beam column element were utilized, respectively. These elements enhance the reliability of structural simulations by capturing the nonlinear response of materials using the plastic hinge approach, providing insights into the performance of structural elements under seismic events. Braces were modelled using displacement-based beam-column elements, which were divided into eight segments to accurately simulate potential plastic behaviour. This approach is deemed more precise compared to modelling the braces as truss elements. To connect the braces to the beams and columns, zero-length elements were utilized representing the localized interactions between the braces and the structural members. A damping ratio of 5% was applied to the superstructure using the Rayleigh damping model (Hammad and Moustafa 2017; Moghaddam, Hajirasouliha, and Doostan 2005) in addition to the effective damping of the base isolation systems, which exceeded 30%. It is worth mentioning that for the seismic isolated projects, the level of dissipated energy due to the damping of superstructure is negligible in comparison with the significant energy dissipation arisen by nonlinear behaviour of seismic isolators (Pant, Wijeyewickrema, and ElGawady 2013). The influence of damping on the seismic response of isolated buildings has been examined in several studies including (Fei et al. 2022; S. Kumar and Kumar 2021; Vu et al. 2014; Zhang et al. 2016)

2.2. Seismic Isolation Systems

To investigate the influence of the proposed 3DSI on the seismic performance of super-structure, the following three different cases were considered:

- (1) Fixed Base (FB).
- (2) Conventional Seismic Isolation (CSI) system, which consists of a lead rubber bearing to provide the horizontal isolation.
- (3) 3DSI, which is a combination of lead rubber bearing and SHDR layers to mitigate the horizontal-vertical responses.

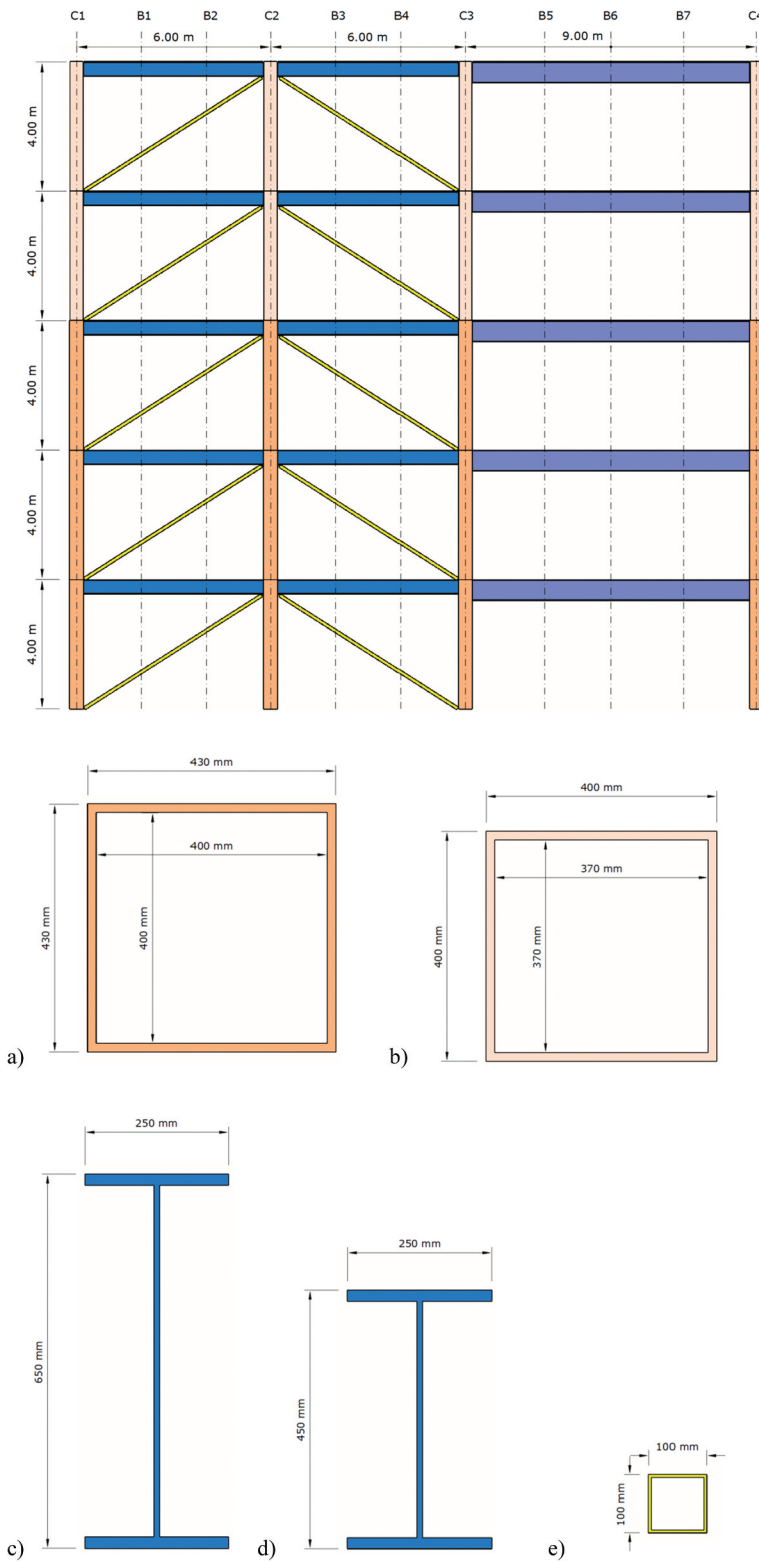


Figure 2. 2D OpenSees model.

In this study, a set of 12 earthquake records obtained from Pacific Earthquake Engineering Research Center online database (PEER NGA) was employed to analyse the structures under coupled horizontal-vertical excitations and extract the structures' responses such as floor acceleration and drift in both directions. Table 1 presents the specifications of the selected ground motions. These 12 nearfield earthquakes are mostly with high vertical peak ground acceleration (PGA), and all were recorded on the sites with soil profiles type C and D in accordance with NEHRP and represent earthquake events with high local magnitudes ($M_s > 6.2$). To cover a variety of vertical peak ground accelerations (PGAs), a wide range of vertical accelerations from 0.27 g to 2.18 g were selected and sorted from the lowest to highest vertical accelerations in this table. To provide more information, the ratios of vertical to horizontal PGAs are also reported, which varied from 30% for Chi-Chi earthquake to over 300% for PRPS excitation.

The unscaled acceleration spectrums in horizontal and vertical directions are illustrated in Fig. 3. This figure also shows the selected Design Basis Earthquake (DBE) and Maximum Considered Earthquake (MCE) acceleration spectrums used to design the conventional isolators. These spectrums correspond to a high seismic region in Wellington, New Zealand.

2.3. Lead Rubber Bearing

Figure 4a,b illustrate the designed Conventional Seismic Isolator (CSI), which consists of 26 rubber layers, each 10 mm thick, and a lead core with a diameter of 170 mm. Figure 4c depicts the combination of the SHDR layers and the conventional LRB mounted on the test machine. The CSI was previously tested under various lateral displacements and compressive loads to evaluate its mechanical properties in the horizontal direction. Figure 5 presents the verification of CSI modelling in OpenSees against experimental test results. The horizontal specifications of the CSI, as derived from the experimental tests, are summarized in Table 2. It can be seen that the adopted model in OpenSees could accurately simulate the cyclic behaviour of the CSI.

According to ASCE 7-22 (2022), the average of the first three cycles was utilized to extract the effective stiffness and effective damping, which led to 0.93 kN/mm and 32% at 310 mm displacement, respectively.

To model the horizontal behaviour of the isolator in OpenSees, the Multilinear Material link was considered to be an ideal option (Vaiana et al. 2021). Each cycle of hysteresis loop was defined by inputting deformation and force (or strain and stress) at each step of the envelope. In this case, three points were introduced to the software to shape the actual bilinear behaviour of LRBs.

Table 1. Specifications of the selected records in this study.

No.	Records	Station	Peak acceleration in H-direction (g)	Peak acceleration in V- direction (g)	Pulse period (s)	V_{PGA}/H_{PGA}	M_w	NEHRP class	$V_{s,30}$ (m/s)
Eq. 1	Christchurch 2011	HVPS**	1.65	2.18	2.65	1.32	6.2	C	422
Eq. 2	Christchurch 2011	PRPS*	0.6	1.9	3.34	3.17	6.2	D	206
Eq. 3	Darfield 2010	GDLC	0.71	1.25	19.8	1.76	7.0	D	344
Eq. 4	Bam 2003	Bam	0.8	0.97	19	1.21	6.6	C	487.4
Eq. 5	Christchurch 2011	Cashmere High school	0.4	0.97	6.3	2.43	6.2	D	204
Eq. 6	Northridge 1994	Rinaldi	0.87	0.96	3	1.1	6.7	D	282.2
Eq. 7	Landers 1992	Lucerne	0.79	0.82	5.1	1.04	7.3	B	1369
Eq. 8	Christchurch 2011	Cathedral	0.38	0.8	5.6	2.11	6.2	D	198
Eq. 9	Christchurch 2011	Hospital	0.35	0.6	7	1.71	6.2	D	194
Eq. 10	Northridge 1994	Sylmar	0.84	0.53	3.1	0.63	6.7	D	251.2
Eq. 11	Kobe 1995	JMA	0.83	0.34	7.8	0.41	6.9	D	312
Eq. 12	Chichi 1999	TCU 065	0.82	0.27	5.7	0.33	7.6	D	305.8

*Pages Road Pumping Station.

**Heathcote Valley Primary School.

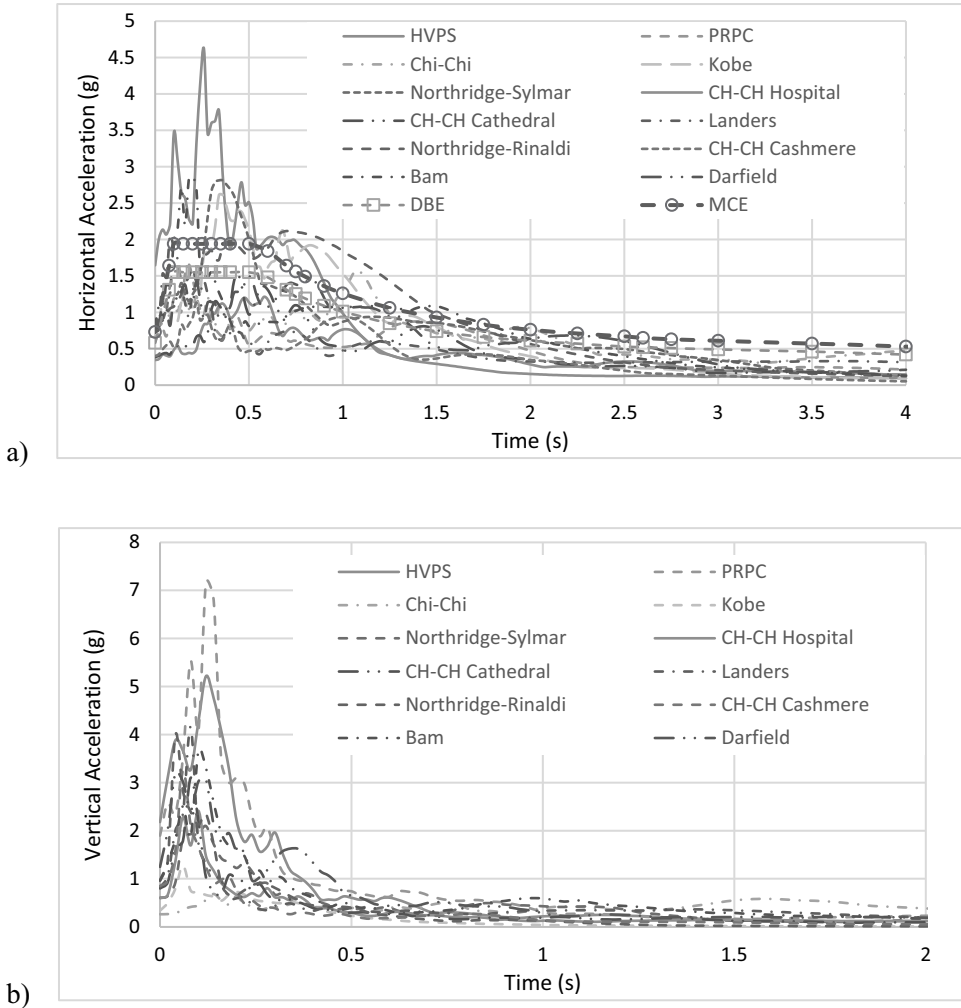


Figure 3. Acceleration response spectra of the selected records. a) horizontal. b) vertical.

It should be noted that modelling and adjusting the vertical specifications of seismic isolators in OpenSees is challenging due to the inherent limitations of predefined isolator elements, such as LeadRubberX and KikuchiAikenLRB, which lack adjustability in the vertical direction. Notably, the vertical characteristics of these predefined isolators are a function of their horizontal attributes, which prevents their independent adjustments. To address this challenge, different elements or materials should be used for the horizontal and vertical directions when modelling a three-dimensional seismic isolator. In this study, Pinching4 Material was utilized to determine the vertical features independently from the horizontal specifications. This material encompasses essential features such as pinching behaviour, strength deterioration, stiffness degradation, and energy dissipation mechanisms, facilitating independent adjustments of LBR specifications in vertical direction.

3. Experimental Tests on SHDR Layers

The vertical effective stiffness of an isolator is a critical factor in mitigating the vertical responses of superstructures, and it is significantly more influential than vertical damping, as shown by Warn and Vu (2012). To determine a practical range of vertical stiffness in this study,

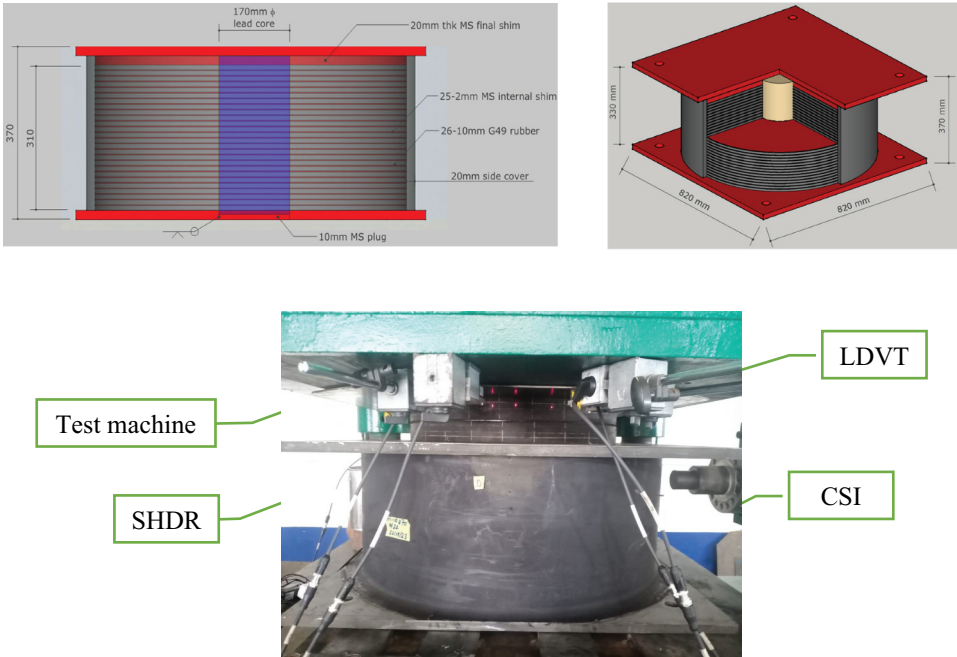


Figure 4. a) The CSI physical specifications, b) CSI's 3D view, c) combined SHDR layer and CSI on the test machine.

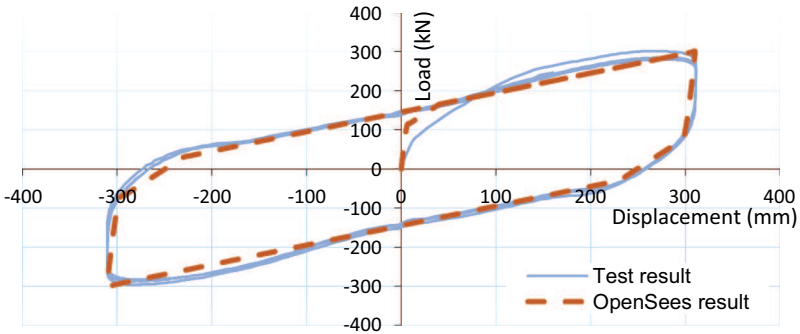


Figure 5. Multilinear material model in OpenSees compared to corresponding test results.

Table 2. The LRB test results.

Cycle	Disp Min (mm)	Disp Max (mm)	Load Min (kN)	Load Max (kN)	Area (kN.m)	k effective (kN/mm)	Damping %
1	-310.1	311.1	-296.0	301.6	185.1	0.962	31.7
2	-310.1	311.1	-287.9	286.2	180.6	0.924	32.2
3	-310.1	311.1	-284.7	280.0	176.9	0.909	32.1

nine SHDR layers were created and tested under cyclic loads. These layers were all 600 mm in diameter and exhibited a high level of damping compared to normal rubber layers. Various thicknesses of 30, 40, and 50 mm, as well as different shear moduli of G60, G80, and G100, were considered. Under 2500 kN cyclic loads, the rubber layers were compressed to investigate their vertical stiffness, bulging, shear strain due to compression, and potential vertical effective

Table 3. SHDR layers' vertical stiffness and compression strain.

Thickness (mm) G modulus (MPa)	Vertical stiffness (kN/mm)			Shear strain due to compression, $\epsilon_{c, E}$		
	50	40	30	50	40	30
G 60	174	331	769	5.2	4.2	3.2
G 80	227	430	997	4.0	3.3	2.5
G 100	276	522	1207	3.3	2.7	2.1

damping. Table 3 presents the dimension and mechanical specification of the SHDR layers under the applied axial load.

The total vertical stiffness of a lead rubber bearing (LRB) at zero displacement is based on the equivalent stiffness of series springs, which is equal to the stiffness of a single layer divided by the number of rubber layers. This stiffness will decrease with increasing lateral displacement and can be calculated using Eqs. (1,2) as presented by Constantinou et al. (2007).

$$K_{V(CSI)} = K_{V0} \left[1 + \frac{3}{\pi^2} \left(\frac{u_h}{r} \right)^2 \right]^{-1} \tag{1}$$

$$K_{V0} = \frac{AE_c}{T_r} \tag{2}$$

where u_h is the lateral displacement, r is the radius of gyration of the bonded rubber area, A is the bonded area of rubber layer, E_c is the compression modulus and T_r is the total thickness of rubber. For the 3DSI device, the vertical stiffness of SHDR layers will be combined with the stiffness gains from Eq. (1) to achieve a low enough stiffness while maintaining the required axial loading capacity.

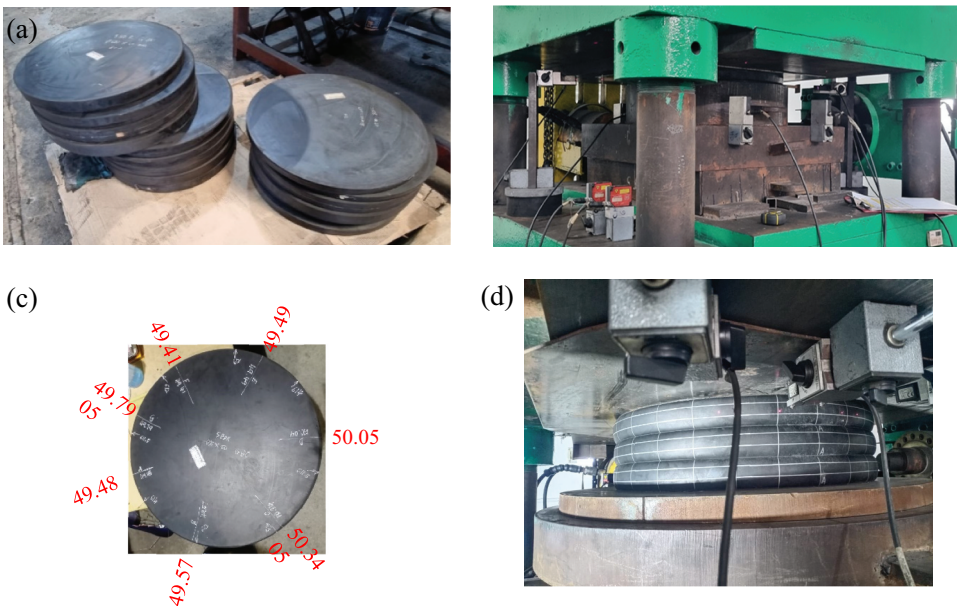


Figure 6. a) The prepared SHDR samples, b) a SHDR layer under the compression loads, c) a SHDR layer after unloading, d) deformation shape of the 3@SHDR.

Figure 6a,b show the prepared SHDR layers and the test rig used to apply cyclic loads. Four Linear Variable Differential Transformers (LDVT) were used to extract the vertical deformations, and one lateral transducer was used to measure lateral bulging. Figure 6c illustrates the measured rubber thickness of a 50-mm-thick SHDR layer at seven spots along the perimeter of the rubber disk after unloading. It was observed that immediately after loading, the original thickness of the rubber was affected by less than 0.3 mm of deformation, demonstrating the acceptable restoring capacity of the SHDR layers. Also, Fig. 6d shows the vertical deformation of the three SHDR layers under compression. As expected, the rubber bulging was uniform around the layers, and no damage or rupture was observed during or after loading.

The vertical stiffness of rubber layers can be calculated using theoretical equations based on the dimensions and stiffness of the rubber. However, stiffness changes due to cyclic loads cannot be predicted by theory alone. Additionally, the calculation of vertical damping and rubber bulging requires data from experimental testing. Therefore, to obtain the practical vertical specifications of rubber in the vertical direction and input them into OpenSees, cyclic axial loading tests are necessary. The test-plan for each layer of the SHDR includes the following three main sections (Table 4):

- (1) Increasing axial load up to 2500 kN for five cycles: In this section, the SHDR layer is subjected to increasing axial loads up to a maximum of 2500 kN. This loading is repeated for five cycles to evaluate the response of the SHDR layer under repeated loading.

Table 4. SHDR axial cyclic test protocol.

Project		3DSI				
Code/Standard		ASCE 07–22				
Isolator Type		SHDR 600 × 30				
PT Parameters						
Diameter (mm)	600	Shape factor (S)	5	Avg. D +0.5 L (kN)	500	
Thickness (mm)	30	G modulus (MPa)	0.6	Max. P1 (kN)	2500	
Kvi (kN/mm)	769.3	Elastic modulus (MPa)	2.12	Max. P2 (kN)	5000	
					Eurocode buckling load, P _{CR} (kN)	18661
Item	Descrip.	Sequence	Axial Load (kN)	Compression strain, ϵ_C	Shear Strain due to compression, $\epsilon_{C,E}$	# Cycles
Cyclic axial test 1						
1	Test 1	Step 1	0	0.022	0.650	10 cycles
		Step 2	2500	0.108	3.250	
Stiffness trend test						
2	Test 2	Step 1	500	0.022	0.650	–
		Step 2	1000	0.043	1.300	–
		Step 3	1500	0.065	1.950	–
		Step 4	2000	0.087	2.600	–
		Step 5	2500	0.108	3.250	–
		Step 6	3000	0.130	3.900	–
		Step 7	3500	0.152	4.550	–
		Step 8	4000	0.173	5.200	–
		Step 9	4500	0.195	5.849	–
		Step 10	5000	0.217	6.499	–
Cyclic axial test 2						
3	Test 3	Step 1	0	0.022	0.650	1 cycle
		Step 2	5000	0.217	6.499	

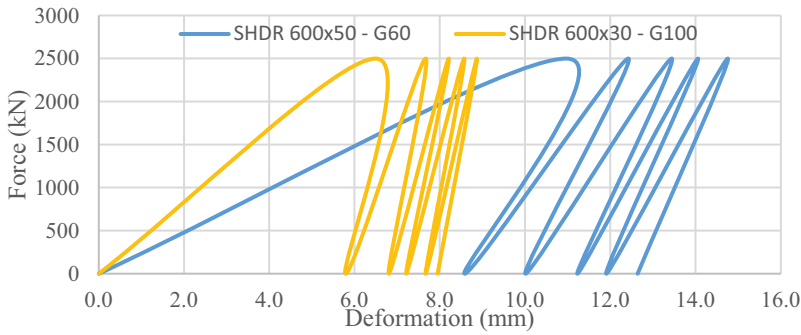


Figure 7. SHDR layers vertical deformations.

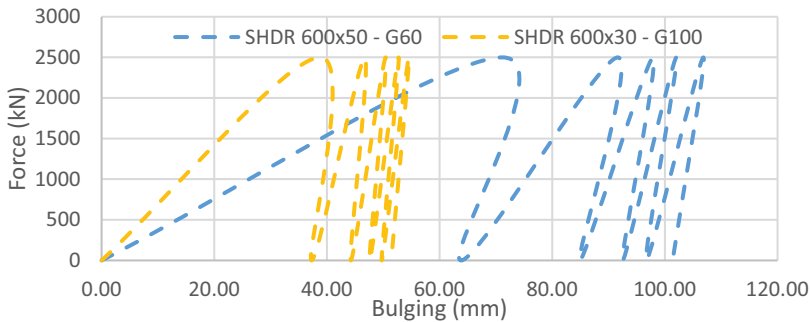


Figure 8. SHDR layers lateral deformations (bulging).

- (2) Increasing axial load step by step up to 5000 kN: This section aims to investigate the rubber bulging behaviour and the vertical stiffness trend under heavy loads. The axial load is increased gradually up to a maximum of 5000 kN. It is important to note that the maximum total design shear strain of a rubber layer should not exceed 7.0. Therefore, the axial loading was avoided to be beyond 5000 kN, as it was the maximum capacity of the test machine and equivalent to 6.5 shear strain.
- (3) Applying the maximum axial load and holding for 30 minutes: In this section, the SHDR layer is subjected to the maximum axial load and held for 30 min for visual inspection. This is to ensure that no damage appears over the rubber surface and to evaluate the long-term performance of the SHDR layer under sustained loading. Figures 7 and 8 display the results from the first five loading cycles of the softest SHDR ($600 \times 50 - G60$) and the stiffest SHDR ($600 \times 30 - G100$). The higher cycles were omitted due to their negligible difference from the fifth cycle. The first loading cycle resulted in 6.5 mm and 11 mm vertical deformation for the hardest and softest SHDRs, respectively. These deformations increased to just below 8 mm and 13 mm after the fifth cycle. Therefore, the vertical stiffness from the first cycle is calculated to be 384 kN/mm and 228 kN/mm for the hardest and softest layers, respectively. In comparison, these values were expected to be about 1207 kN/mm and 174 kN/mm based on theory, which presents a significant difference in the case of stiffer layer. It should be noted that, since the vertical deformations are usually small amounts (particularly compared to horizontal displacement), the rubber vertical stiffness is highly sensitive to variation of vertical deformation, and even a few millimetres of deformation variation might change the expected stiffness considerably. On the other hand, rubber is naturally an incompressible material, in which even identical pairs do not necessarily have precisely similar specifications. Therefore, to achieve reliable designs,

Table 5. SHDR 600 × 50 – G60 test results.

Cycle		Deformation (mm)	Bulging (mm)	K_v (kN/mm)	T_v (s)	ϵ_c	ϵ_{sc}	EDC (kN.mm)	β
SHDR (1 layer)									
1	0	0.00	0.00	228.05	0.21	0.22	3.9	10728.125	24.9%
	2500	10.96	71.18						
2	0	8.58	63.81	651.47	0.12	0.08	1.4	1784.375	11.8%
	2500	12.42	91.63						
3	0	10.01	84.90	728.86	0.12	0.07	1.2	1521.875	11.3%
	2500	13.44	97.91						
Ave.				536.13	0.14				

Table 6. SHDR 600 × 30 – G100 test results.

Cycle		Deformation (mm)	Bulging (mm)	K_v (kN/mm)	T_v	ϵ_c	ϵ_{sc}	EDC (kN.mm)	β
SHDR (1 layer)									
1	0	0.00	0.00	384.62	0.16	0.22	6.5	7240.625	28.4%
	2500	6.50	38.83						
2	0	5.79	37.27	1333.33	0.09	0.06	1.9	1262.5	17.1%
	2500	7.67	46.73						
3	0	6.80	44.26	1776.20	0.08	0.05	1.4	512.5	9.3%
	2500	8.21	50.43						
Ave.				1164.72	0.09				

Table 7. Vertical stiffness and period for three layers of SHDR 600 × 50 - G60, and the proposed 3DSI.

	SHDR (3 layers)		3DSI	
	$K_v - 3@SHDR$ layers	$T_v - 3@SHDR$ layers	K_{3DSI}	$T_{V(total)}$
1	76.02	0.36	59.88	0.41
2	217.16	0.22	122.70	0.29
3	242.95	0.20	130.53	0.28
Ave.	178.71	0.24	K_{3DSI} 104.37	T_{V-3DSI} 0.31

Table 8. Vertical stiffness and period for the three layers of SHDR 600 × 30– G100, and the proposed 3DSI.

	SHDR (3 layers)		3DSI	
	$K_v - 3@SHDR$ layers	$T_v - 3@SHDR$ layers	K_{3DSI}	$T_{V(total)}$
1	128.21	0.28	88.14	0.34
2	444.44	0.15	172.56	0.24
3	592.07	0.13	191.05	0.23
Ave.	388.24	0.16	K_{3DSI} 150.58	T_{V-3DSI} 0.26

Table 9. CSI vertical stiffness at zero and maximum displacement.

E_c (MPa)	A (mm ²)	Tr (mm)	u (mm)	r	K_{v0} (kN/mm)	K_v (kN/mm)
658	418539	260	310	182.50	1059.26	282.07

the design targets need to be based on experimental outputs through practical tests. In the lateral direction, due to the incompressibility of rubber, the compressed volume bulged from the perimeter area of the rubber, which was about 51 mm and 101 mm for the hardest and softest layers, respectively.

Tables 5 and 6 list the vertical specifications of SHDR $600 \times 50 - G60$ and SHDR $600 \times 30 - G30$. The vertical period (T_v), compression strain (ϵ_c) and shear strain due to compression load (ϵ_{sc}), energy dissipation per cycle (EDC) and effective damping (β) are reported. It is observed that SHDR 600×50 has a higher vertical period and lower shear strain in comparison with SHDR 600×30 . The extracted shear strain of SHDR 600×50 is just below 4.0, which is conservatively below 7.0 as the maximum shear strain recommended by BS EN 15129 (2018). The effective damping in the vertical direction is not as influential as vertical stiffness; however, other researchers reported that 20% vertical damping is acceptable (Eltahawy et al. 2018). In this case, 25% and 28% vertical damping were achieved from the softest and hardest layers, respectively. To obtain a suitable 3DSI system in this study, it was decided to use three layers of SHDR. Therefore, the device's total vertical stiffness was calculated based on the vertical stiffness of CSI at maximum displacement and the vertical stiffness of three layers of SHDR. Tables 7 and 8 demonstrate that the vertical stiffness and vertical period values obtained from combining SHDR layers and the CSI. Eq. 1 and Eq. 2 were utilized to obtain the CSI vertical stiffness using the isolator specifications shown in Fig. 4c. Table 9 presents the CSI vertical stiffness at zero and maximum displacement. Based on the presented results, the dominant vertical period is around 0.41 s and 0.34 s for the softest and stiffest layers, respectively. ASCE 7-22 (2022) recommends considering the average of the first three cycles to match the isolator's characteristics with the design target. Therefore, to define the effective stiffness of the 3DSI in OpenSees, the average stiffness from the first three cycles of SHDR 600×50 combined with the CSI vertical stiffness at the designed maximum displacement was employed.

As discussed before, given the hysteresis loops obtained from the SHDR tests, it was realized that Pinching4 material suits to model the vertical response in OpenSees. This material considers the degradation under cyclic loads and exhibits the "pinched" load-deformation behaviour. Figure 9 illustrates the vertical stiffness diagram of the assumed isolator. Figure 9a shows the compression and tension behaviour of the 770LRB170 attained from the experimental test, where the compression and tension stiffness are depicted in positive and negative, respectively. As expected, the LRB is significantly stiffer under the compression loads than the tension loads. Generally, the LRBs stiffness under the tension loads are $1/20$ to $1/50$ softer than the compression loads (Pietra and Park 2016). Figure 9b demonstrates the SHDR hysteresis loops under the compression load gained from the test. It should be noted that since the SHDR layers are not supposed to take tension actions, only the compression stiffness is shown in this figure. Figure 9c exhibits the equal stiffness of the assumed 3DSI to define in OpenSees software based on the combination of Fig. 9a,b. This diagram indicates that the 3DSI compression stiffness is efficiently dropped to one-tenth of the CSI compression stiffness. In addition, the dissipated energy area under the compression loop (area under the curve in a plot of force versus displacement) indicates that the 3DSI isolators provide a certain degree of vertical damping. It is notable that, the compression stiffness of a CSI unit normally is considerably more than its tension stiffness, while, the proposed 3DSI, offers the compression stiffness even below the tension stiffness.

4. Assessment of the Selected Records

Adopting a suitable intensity measure (IM) to scale near-fault earthquakes for base-isolated buildings can be a complex task, as there are a variety of approaches to determining strong-velocity pulses in near-field earthquakes (Mazza and Labernarda 2017). This study utilized the unscaled ground motions since they were used to compare the performance and floor acceleration of the assumed seismic isolation system instead of designing the superstructure.

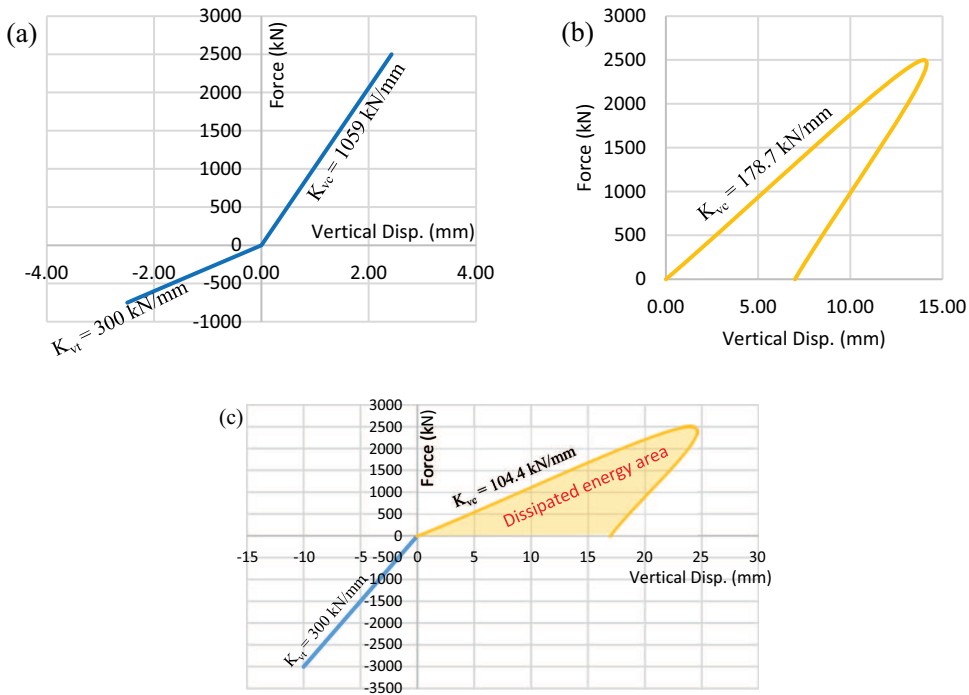


Figure 9. Vertical stiffness: a) CSI, b) SHDR 600 × 50-G60, c) 3DSI.

Figure 10a demonstrates the vertical elastic response spectrum for the chosen seismic excitations, range from 0 to 0.8 s. This figure illustrates that the vertical periods around 0.1 s, which represent the vertical period of most conventional isolators, might magnify the vertical acceleration to more than 5.0 g, leading to extensive non-structural damage. It should be noted that vertical accelerations less than 1.0 g are not generally harmful to non-structural elements, while accelerations between 1.0 and 2.0 g can cause shaking of objects and once the vertical acceleration goes beyond 2.0 g, tossing and falling of the objects will be expected (Guzman, Jean, and Ryan 2018). Therefore, increasing the vertical period up to more than 0.3 s significantly decreases the acceleration below 2.0 g regardless of the vertical damping influence. Figure 10b illustrates that by increasing the vertical periods beyond 0.3 s and 20% damping, the corresponding acceleration will be degraded to less than 1.0, even for those two records with the highest vertical PGA.

5. Discussion and Results

The aim of this section is to investigate the influence of the 3DSI on the building's responses and compare them with the Conventional Seismic Isolators (CSI) and Fixed Base (FB) options.

Tables 10–12 presents the vertical accelerations (VA) at the locations of columns and the beams as illustrated in Fig. 2. For each structural system, the accelerations at each column, two spots on the 6 m beams, and three spots on the 9 m beams were considered. In these tables, accelerations less than 2.0 g are highlighted in green, accelerations up to 4.0 g and 5.0 g are shown in yellow and orange, respectively, and any acceleration exceeding 5.0 g is presented in light red. As it was expected, the fixed base option resulted in vertical accelerations to gradually increase from bottom to top of columns as well as from end of the beams toward the centre of the beams.

Table 10 presents negligible difference between the VA values on the ground level and the roof level on the location of columns, while the amplification was more than 300% from the ground level to the

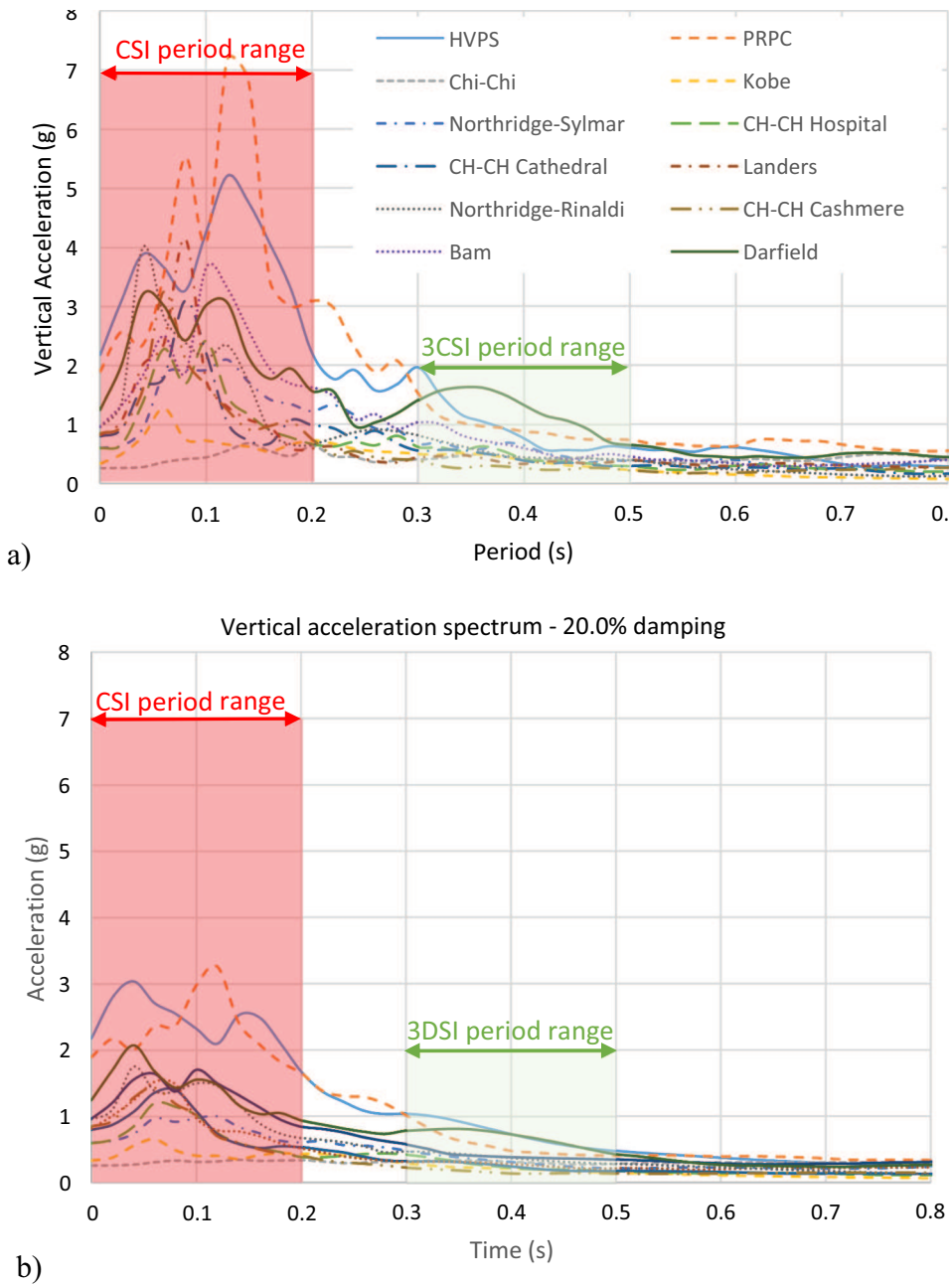


Figure 10. Vertical response spectrum for 12 selected ground excitations: a) 5% damping, b) 20% damping.

middle of the 9 m beam. This table shows that although the fixed base building is vertically rigid, the emerged vibration along with the beams, particularly for the long span beams, can result in high vertical accelerations and correspondingly non-structural damage. This confirms the importance of considering the vertical component of earthquake for seismic design and assessment of buildings in near field zones.

Table 10. Vertical accelerations of columns and beams for the fixed base option – HVPS record.

Story	C1	B1	B2	C2	B3	B4	C3	B5	B6	B7	C4
Fixed Base (FB) – Vertical ACC (g)											
ST 5	2.1	5.6	5.9	2.6	5.3	5.1	2.4	4.8	6.6	4.3	3.2
ST 4	2.0	4.0	4.5	2.4	4.9	4.8	2.3	5.1	7.0	5.0	3.1
ST 3	1.9	4.0	4.4	2.1	3.7	3.6	2.0	3.8	5.3	4.3	2.9
ST 2	1.9	3.2	3.5	1.7	3.2	3.0	1.9	2.9	4.3	2.9	2.5
ST 1	1.9	2.6	2.6	1.7	2.7	2.8	1.7	3.9	5.0	3.3	2.2
G.F.	2.1			2.1			2.1				2.1

Table 11. Vertical accelerations of columns and beams for the 3DSI option – HVPS record.

Story	C1	B1	B2	C2	B3	B4	C3	B5	B6	B7	C4
Three-Dimensional Seismic Isolation (3DSI) – Vertical ACC (g)											
ST 5	1.6	2.2	2.1	1.7	2.3	2.3	1.8	2.5	3.3	2.9	2.2
ST 4	1.6	2.0	2.2	1.6	2.1	2.1	1.8	1.9	2.7	1.9	2.2
ST 3	1.5	2.0	2.2	1.5	2.0	1.9	1.7	1.8	2.6	2.2	2.1
ST 2	1.5	1.9	2.0	1.5	1.9	2.0	1.7	1.7	2.4	2.1	2.1
ST 1	1.5	1.9	1.8	1.5	1.9	2.0	1.7	1.7	2.5	2.1	2.0
Tl. *	1.6			1.6			1.8				2.1
Bl. **	2.2			2.2			2.2				2.2

*Top of Isolation level.

**Bottom of Isolation level.

Table 12. Vertical accelerations of columns and beams for the CSI option – HVPS record.

Story	C1	B1	B2	C2	B3	B4	C3	B5	B6	B7	C4
Conventional Seismic Isolation (CSI) – Vertical ACC (g)											
ST 5	4.6	4.7	5.2	4.2	4.6	5.1	4.6	6.6	9.3	7.0	4.7
ST 4	4.4	4.4	4.8	4.0	4.6	5.5	4.5	5.0	6.7	5.4	4.6
ST 3	4.0	4.3	5.0	3.8	4.6	4.9	4.2	5.0	6.7	5.3	4.3
ST 2	3.9	4.0	4.6	3.6	4.3	4.6	3.8	4.3	5.8	4.4	4.1
ST 1	4.0	3.9	4.2	3.9	4.0	4.3	3.8	4.8	6.4	5.3	4.1
Tl. *	3.9			3.9			4.2				4.7
Bl. **	2.2			2.2			2.2				2.2

The CSI option led to amplification of vertical PGA due to low vertical flexibility of isolators, which magnified the accelerations from the bottom to the top of the device. In this case, the VA values on the columns are almost twice as the VAs attained from the fixed base option. For better comparison, Table 11 demonstrates that the CSI units almost doubled the vertical PGA on the isolation level, which resulted in considerable escalation of responses on the middle of beams specifically for the long spans. The results show that on the roof level, the VA has increased from 6.6 g for the fixed base to 9.3 g for the seismic isolated option, representing a 40% increase.

Table 12 shows that unlike the CSI option, three-dimensional isolation could effectively decrease the vertical accelerations. In this case, the VA decreased from 3.9 g to 1.6 g on top of the C1 isolation and from 9.3 g to 3.3 g in the middle of the long beam, undermining the non-structural damage level. Notably, in the case of the three-dimensional isolator, besides the 3.3 g acceleration in the middle of

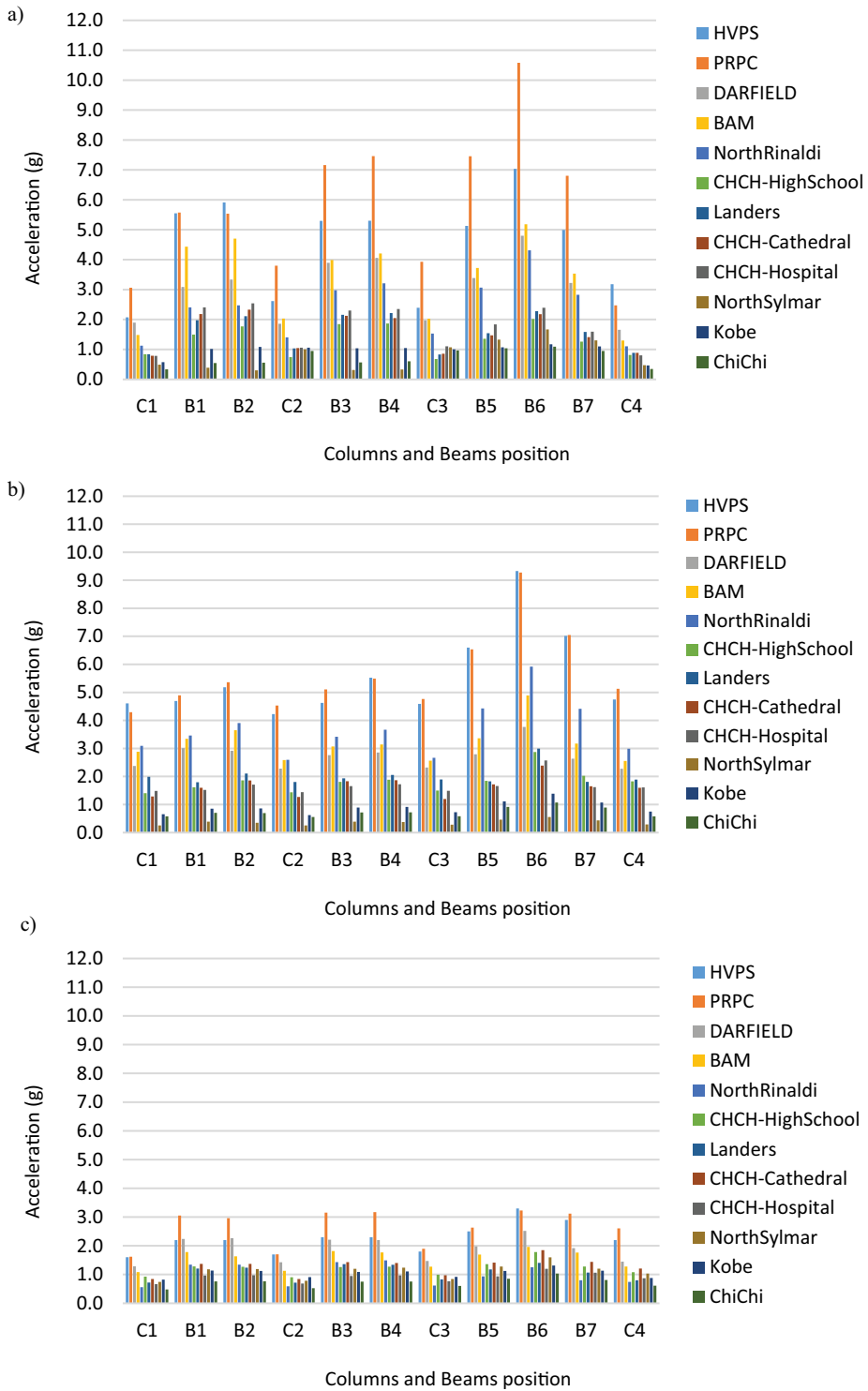
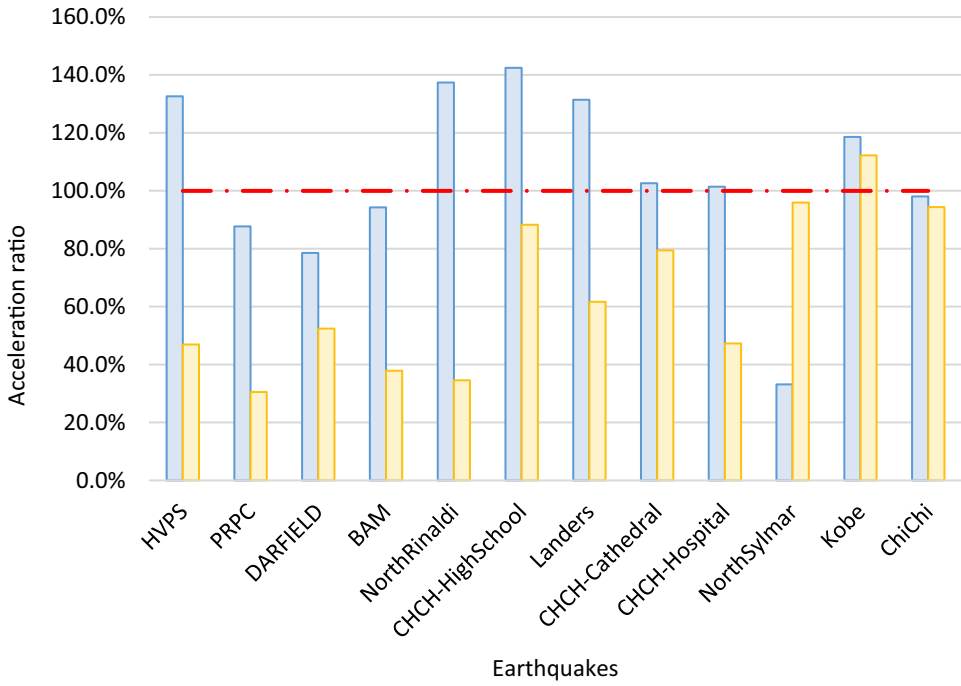


Figure 11. Maximum vertical accelerations at the position of columns of beams for each earthquake. a) fixed base, b) Conventional Seismic Isolation, c) three-dimensional Seismic Isolation.



CSI/F.B. 3DSI/F.B. - - - 100%

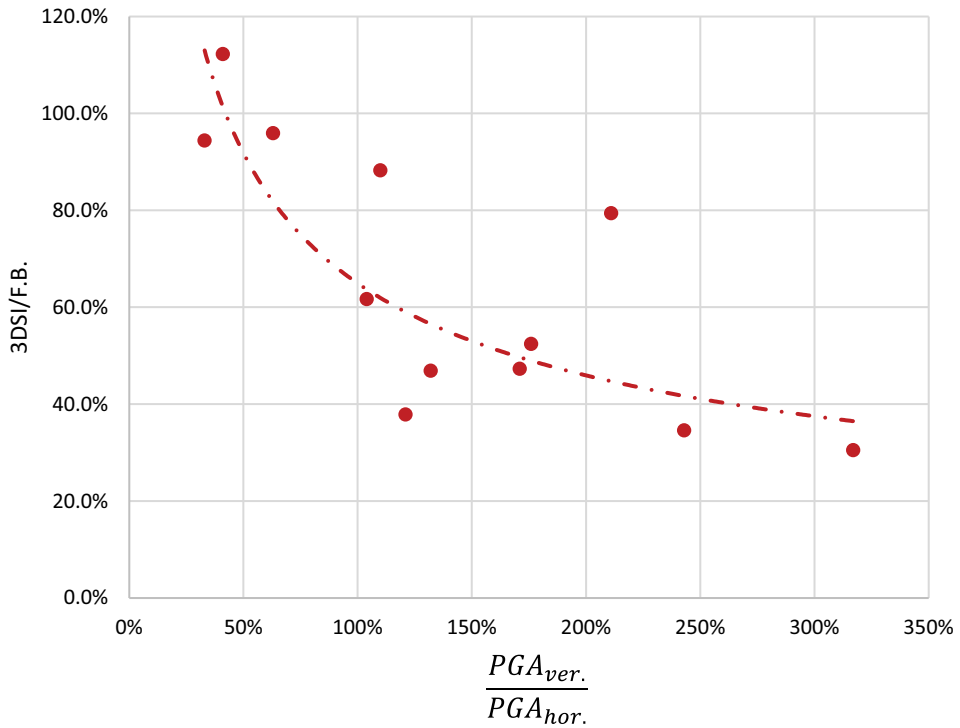


Figure 12. a) Efficiency of 3DSI vs CSI. b) 3DSI efficiency trend vs Ver./Hor. PGA ratio.

the long beam, other values predominantly remain at around 2.0 g, indicating potential shaking of objects and furniture in a worst-case scenario rather than being tossed around.

Figure 11 demonstrates the maximum vertical acceleration of the floors under all excitations. Figure 11a shows the respond of the fixed base system to the coupled horizontal vertical excitations, while Fig. 11b,c represent the conventional and three-dimensional seismic isolation, respectively. These figures highlight the following observations:

- (i) The vertical acceleration at the midspan of the long beam (B6) exceeded 1.0 g for all excitations, demonstrating the influence of beam span on vibration amplification.
- (ii) Even for earthquakes with low vertical PGA, the vertical acceleration ratio was 3–4 times greater than the vertical PGA for both the FB and CSI systems. The highest vertical amplification was observed for the CSI system under the Northridge earthquake, where a vertical PGA of 0.97 g escalated to over 5.9 g at the position of B6—an amplification exceeding 600%.
- (iii) For the FB and CSI systems, complete non-structural damage thresholds are expected under HVPS and PRPC excitations, as vertical accelerations exceeded 5 g. For other earthquakes, such as Darfield, Bam, Northridge, and Christchurch, where vertical accelerations ranged between 2 g and 5 g, damage levels are projected to range from medium to extensive.
- (iv) The 3DSI system effectively reduced vertical accelerations, particularly for high vertical PGA events. For instance, under PRPC excitation, the maximum vertical acceleration was limited to 3.0 g, which is approximately one-third of the maximum acceleration observed in the CSI system and less than half of that in the FB system.

Figure 12 highlights the efficiency of the 3DSI system compared to the CSI system. Figure 12a illustrates the ratio of vertical accelerations of the isolation systems relative to the fixed-base (Efficiency Ratio) option. The results show that, for most earthquakes, the CSI system resulted in similar (approximately 100%) or higher (greater than 100%) vertical accelerations compared to the FB system. The maximum ratio was observed for the Christchurch High School station, where the ratio exceeded 140%. In contrast, the 3DSI system significantly reduced the acceleration ratio. Notably, for the five earthquakes with the highest vertical PGA, the acceleration ratio was approximately 40%, highlighting the necessity of three-dimensional seismic isolation in near-field zones.

Figure 12b illustrates the trend of the 3DSI efficiency ratio relative to the vertical-to-horizontal PGA ratio. This figure indicates that the efficiency of the 3DSI system increases for earthquakes with high vertical PGAs. In other words, maximum acceleration attenuation is expected at stations with a higher vertical-to-horizontal PGA ratio.

To further evaluate the efficiency of the proposed isolation system for multistorey buildings along their height and length, Fig. 13 illustrates the distribution of acceleration along the beams at two different levels. Figure 13a compares the HVPS results at levels 1 and 5, showing that the 3DSI system effectively reduces accelerations to below the vertical PGA (2.20 g) at the column positions, achieving approximately a 30% reduction. In contrast, the FB option slightly increases the column responses, while the CSI option approximately doubles them. The 3DSI system results in an almost uniform distribution of acceleration across the beam, with negligible amplification at the beam's centre, unlike the other two options. This implies minimal seismic deformation at the beam-column joints. In contrast, the CSI option produces the highest acceleration at the centre of long beams, while the FB option generates higher accelerations on short beams.

Figure 13b illustrates the average of maximum vertical responses across all excitations. Notably, the average maximum accelerations are limited to approximately 2.0 g, which is the threshold for damage to non-structural elements. As a result, the use of the proposed 3DSI system is expected to lead to none to slight damage to non-structural components. Additionally, the 3DSI system effectively minimizes the destructive influence of long beams on acceleration amplification. This performance is attributed to the system's appropriately designed vertical period, which is a critical factor in bypassing the short-period range of the acceleration spectrum.

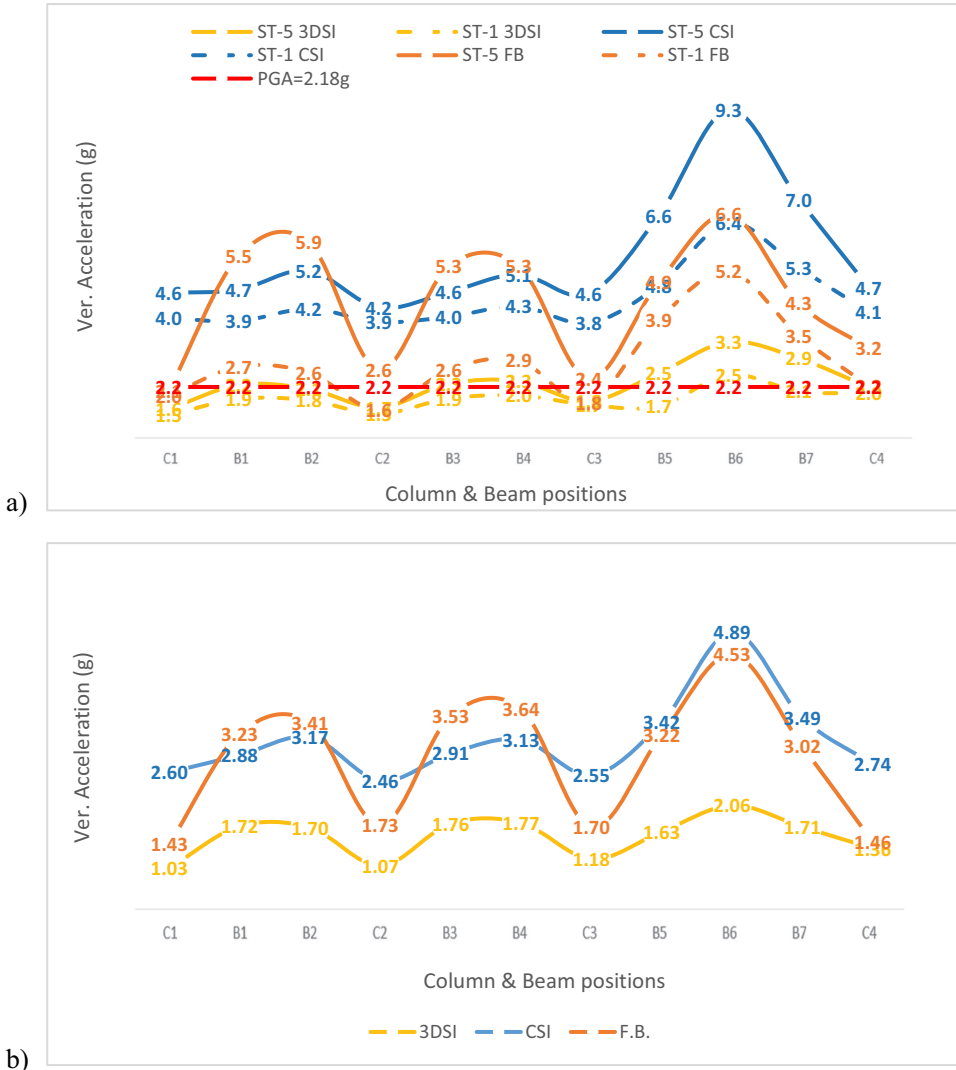


Figure 13. Vertical acceleration distribution of columns and beams at levels 1 and 5: a) HVPS, b) average of maximum accelerations of all records.

Figure 14 illustrates the trend of acceleration variation along the height in the horizontal direction. It demonstrates that, on average, floor horizontal accelerations are significantly reduced for both the CSI and 3DSI systems compared to the FB option. In the figure, the green area represents the recommended horizontal acceleration range to limit non-structural damage to a slight level, while the yellow and red areas indicate medium to extensive non-structural damage (FEMA 2003). The results clearly show that the 3DSI system is more effective at attenuating horizontal accelerations than the CSI option. It is worth noting that the impact of vertical excitations on horizontal responses and the rationale behind the amplification of vertical accelerations by conventional isolators are discussed in detail by Pourmasoud et al. (2020).

Figures 15 and 16 depict the axial and lateral forces of the first floor columns under HVSC ground motion (with highest vertical PGA) and the average of axial and lateral forces from all excitations, respectively. Figure 15a and 16a display the compression and tension responses for each system, while Figs. 15b and 16b compare the columns' base shear. The results in Fig. 15 demonstrates that the use of

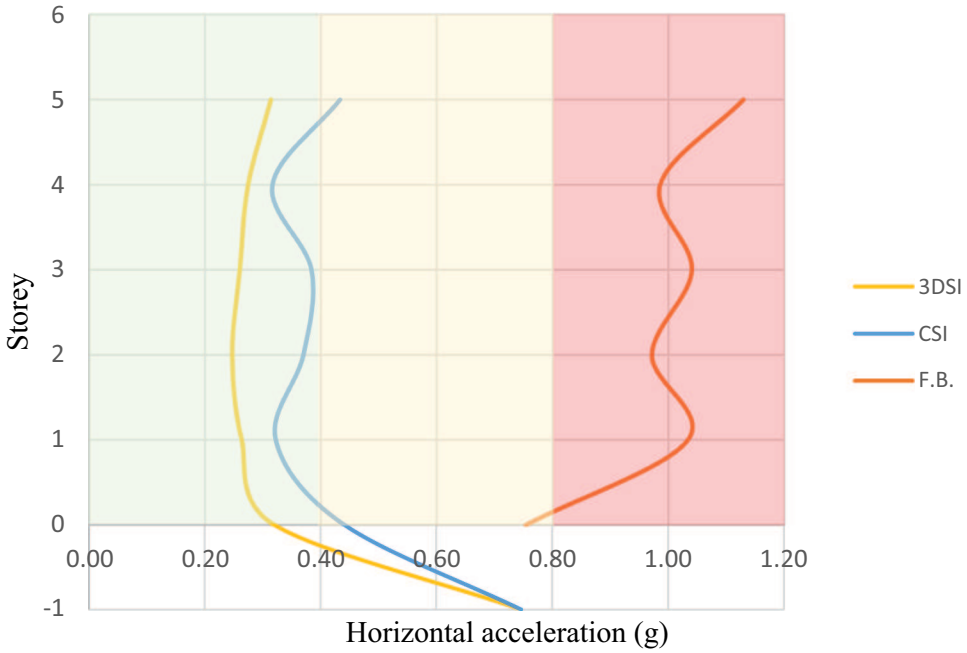


Figure 14. Horizontal acceleration distribution along with the height.

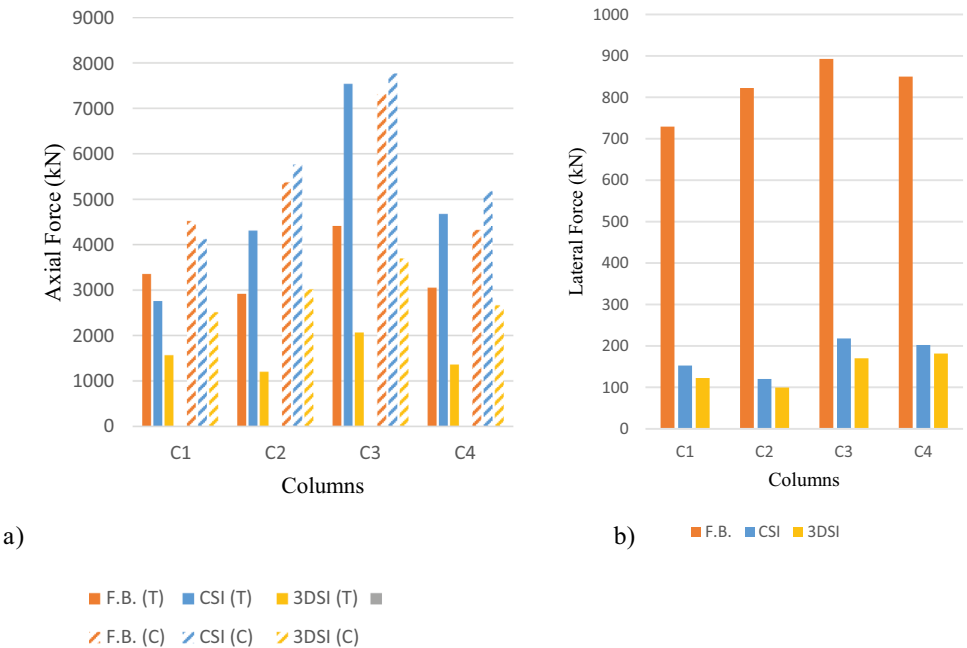


Figure 15. HVSC ground motion. a) columns' axial load. b) columns' base shear.

the CSI system significantly reduces the lateral forces; however, due to the partial vertical flexibility of isolators and the extreme vertical PGA of the HVSC record, the axial loads of columns remained similar or slightly increased compared to the fixed base (FB) option. The 3DSI system significantly

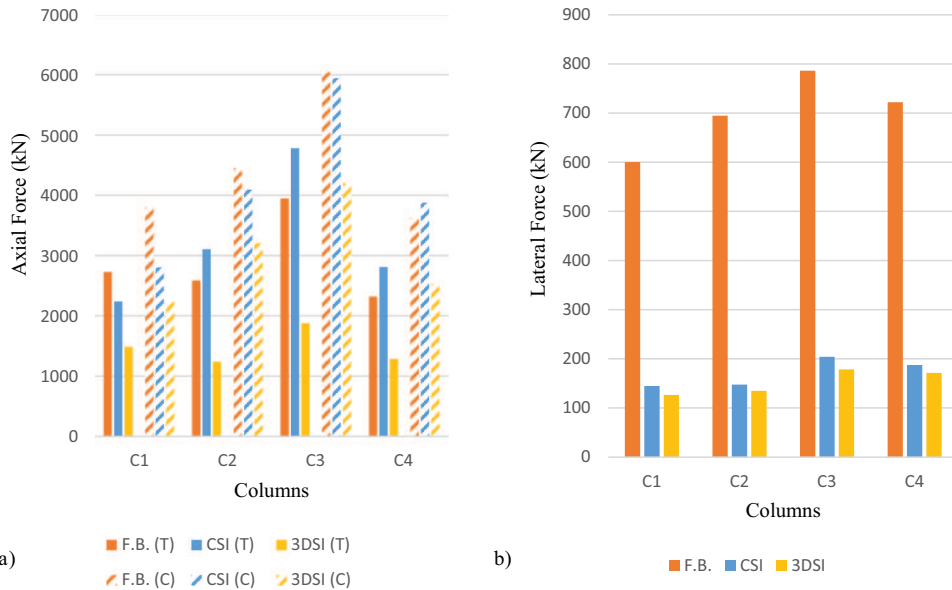


Figure 16. a) Average of columns' axial loads from all excitations, b) average of columns' shear forces from all excitations.

Table 13. Story drifts under HVSC excitation.

HVSC	St.	1	2	3	4	5
	3DSI	0.0013	0.0016	0.0014	0.0012	0.0008
	CSI	0.0014	0.0019	0.0015	0.0016	0.0017
	FB	0.0102	0.0147	0.0114	0.0075	0.0033

Table 14. Average story drifts due to all records.

Average.	St.	1	2	3	4	5
	3DSI	0.0014	0.0016	0.0013	0.0011	0.0008
	CSI	0.0013	0.0017	0.0013	0.0013	0.0011
	FB	0.0103	0.0113	0.0071	0.0041	0.0022

decreases the compression and tension forces under the coupled horizontal-vertical HVSC excitation, reducing the maximum compression and tension loads from over 7000 kN to less than 4000 kN and 2000 kN, respectively. In the horizontal direction, the maximum lateral base shear is reported to be approximately 900 kN for the fixed base option. However, this value decreases to 220 kN and 170 kN for the CSI and 3DSI systems, respectively. Notably, although the horizontal specifications of both isolation systems are the same, the horizontal responses of the proposed system are approximately 20% less than those of the conventional isolation system. The same trend is observed for the average of all records, while the CSI system leads to a considerable decrease in lateral forces compared to the fixed base option, and the compression/tension forces vary up to $\pm 10\%$. It can be also seen that, on average, the 3DSI system reduces the compression loads by 25% and the tension loads by 50% compared to the CSI system.

To assess the expected damage in different systems, the story drift values were compared with the thresholds of non-structural damage according to (FEMA 2003). It is worth noting

that the nature of damage due to acceleration is different from the damage caused by floor drift. Acceleration causes objects to be tossed or fall directly, while non-structural drift damages are due to inelastic deformation of ductile elements and connections, which affect non-structural elements such as ceilings and partitions. Floor drifts up to 0.008, cause slight damage, while moderate damage occurs when they exceed 0.008. On the other hand, extensive damage is expected to occur when the floor drift exceeds 0.025. Tables 13 and 14 compare the story drift values of the 3DSI system with the other two systems under the HVSC excitation and the average of all excitations. Both isolation systems resulted in a small amount of floor drift, reasonably below the slight threshold. However, the fixed base option exhibited considerably higher floor drift values, which is expected to cause moderate to extensive damage to non-structural elements. Table 14 shows that the drift ratio of a fixed base building, particularly in the first floors, can be up to seven times more than that of base-isolated buildings, which increases the non-structural damage threshold from slight to extensive level.

6. Summary and Conclusions

While Conventional Seismic Isolation (CSI) systems are highly effective at mitigating seismic responses of structures in the horizontal direction, their ability in the vertical direction is limited. To address this issue, in this study the performance of a new Three-Dimensional Seismic Isolator (3DSI) was investigated both experimentally and analytically. In the proposed system, the vertical isolation was achieved by using Super-High-Damping-Rubber (SHDR), which reduces vertical effective stiffness and increases vertical effective damping, thus minimizing the imparted vertical acceleration into the superstructure. Three case-study buildings, including 5-story steel frames with Fixed Base (FB), Conventional Seismic Isolators (CSI), and the proposed 3DSI, were analyzed subjected to 12 earthquake records using OpenSees software with experimentally validated models. Based on the presented results, the following conclusions can be drawn:

- (1) CSI systems have low vertical flexibility, leading to amplification of vertical excitations along the height and middle of beams, resulting in vertical accelerations that can be twice as high as those experienced by FB buildings.
- (2) The proposed 3DSI system attenuated vertical accelerations by up to 65% compared to the CSI system, resulting in lower levels of non-structural damage. The trend of vertical accelerations along the height showed an escalation trend for FB and CSI systems, while the 3DSI system led to a more uniform distribution of vertical accelerations along the height.
- (3) Both CSI and 3DSI systems significantly reduced the lateral forces on columns compared to FB buildings. The 3DSI system offered 20% less lateral forces than the CSI system and approximately 50% and 25% less compression and tension axial loads, respectively.
- (4) CSI and 3DSI systems resulted in similar story drifts, less than the slight damage level proposed by FEMA, while the fixed-base option exhibited higher story drifts, particularly for the first two stories beyond the extensive non-structural damage.

Overall, this research demonstrates that the proposed 3DSI system is highly effective in reducing the seismic responses of buildings compared to FB and CSI options, despite potential epistemic uncertainties in numerical studies. The system provides an enhanced level of safety for building occupants and equipment, making it a compelling choice for seismic isolation in near-field zones with high vertical PGAs. Notably, the 3DSI system is tunable in both horizontal and vertical directions to meet specific project requirements. In this study, a vertical period of $T_v = 0.3s$, was targeted, effectively mitigating coupled horizontal-vertical responses. A longer vertical period can be achieved by adjusting the specifications and number of SHDR layers.

Acknowledgments

Special thanks to those have assisted to this research, in particular the technical support from Low Damage Design Co.

Disclosure Statement

No potential conflict of interest was reported by the author(s).

ORCID

Iman Hajirasouliha  <http://orcid.org/0000-0003-2597-8200>

References

- ASCE 7-22. 2022. *Minimum Design Loads and Associated Criteria for Buildings and Other Structures*. LCCN 20170182751. Virginia, USA: American Society of Civil Engineers.
- BS EN 15129. 2018. *European Standard on Anti-Seismic Devices*. Bruxelles: BSI Standard Publication.
- Cancellara, D., and F. De Angelis. 2016. "Nonlinear Dynamic Analysis for Multi-Storey RC Structures with Hybrid Base Isolation Systems in Presence of Bi-Directional Ground Motions." *Composite Structures* 154 (October): 464–492. <https://doi.org/10.1016/j.compstruct.2016.07.030>.
- Cao, Y., P. Peng, H. Wang, J. Sun, G. Xiao, and Z. Zuo. 2023. "Development of an Innovative Three-Dimensional Vibration Isolation Bearing." *Engineering Structures* 295 (November): 116890. <https://doi.org/10.1016/j.engstruct.2023.116890>.
- Cimellaro, G. P., M. Domaneschi, and G. Warn. 2018. "Three-Dimensional Base Isolation Using Vertical Negative Stiffness Devices." *Journal of Earthquake Engineering* 24 (12): 2004–2032. August. <https://doi.org/10.1080/13632469.2018.1493004>.
- Constantinou, M. C., A. S. Whittaker, Y. Kalpakidis, D. M. Fenz, and G. P. Warn. 2007. *Performance of Seismic Isolation Hardware Under Service and Seismic Loading*. MCEER-07-0012. Buffalo, NY: Multidisciplinary Center for Earthquake Engineering Research (MCEER).
- Dong, W., Y. Shi, Q. Wang, Y. Wang, and J.-B. Yan. 2023. "Development of a Long-Period Vertical Base Isolation Device with Variable Stiffness for Steel Frame Structures." *Soil Dynamics and Earthquake Engineering* 164 (January): 107638. <https://doi.org/10.1016/j.soildyn.2022.107638>.
- Eltahawy, W., K. L. Ryan, S. Cesmeçi, and F. Gordaninejad. 2018. "Parameters Affecting Dynamics of Three-Dimensional Seismic Isolation." *Journal of Earthquake Engineering*: 1–26. <https://doi.org/10.1080/13632469.2018.1537902>.
- Fei, Y.-F., Y. Tian, Y. Huang, and X. Lu. 2022. "Influence of Damping Models on Dynamic Analyses of a Base-Isolated Composite Structure Under Earthquakes and Environmental Vibrations." *Gong Cheng Li Xue/Engineering Mechanics* 39 (March): 201–211. <https://doi.org/10.6052/j.issn.1000-4750.2021.07.0500>.
- FEMA. 2003. *Multi-Hazard Loss Estimation Methodology - Earthquake Model*. HAZUS-MH MR4 Technical Manual. Washington: Federal Emergency Management Agency.
- FEMA E-74. 2012. "FEMA E-74, Reducing the Risks of Nonstructural Earthquake Damage | Fema.Gov 2012." <https://www.fema.gov/emergency-managers/risk-management/earthquake/training/fema-e-74>.
- Fujita, T., S. Fujita, Y. Watanabe, A. Kato, S. Suzuki, and K. Fukumori. 1996. "Fundamental Study of Three-Dimensional Seismic Isolation System for Nuclear Power Plants." In *Proceedings, 11th World Conference on Earthquake Engineering*. Acapulco, Mexico: Elsevier Science.
- Furukawa, S., E. Sato, Y. Shi, T. Becker, and M. Nakashima. 2013. "Full-Scale Shaking Table Test of a Base-Isolated Medical Facility Subjected to Vertical Motions." *Earthquake Engineering & Structural Dynamics* 42 (13): 1931–1949. <https://doi.org/10.1002/eqe.2305>.
- Gu, Z., X. Wu, L. Feng, Y. Sun, Z. Cheng, W. Qian, and H. Gong. 2024. "Seismic Response Analysis and Damage Calculation of Long-Span Structures with a Novel Three-Dimensional Isolation System." *Buildings* 14 (6): 1715. <https://doi.org/10.3390/buildings14061715>.
- Guzman, P., C. Jean, and K. L. Ryan. 2018. "Computational Simulation of Slab Vibration and Horizontal-Vertical Coupling in a Full-Scale Test Bed Subjected to 3D Shaking at E-Defense." *Earthquake Engineering & Structural Dynamics* 47 (2): 438–459. <https://doi.org/10.1002/eqe.2973>.
- Hammad, A., and M. A. Moustafa. 2017. "Seismic Performance of Braced Steel Frames Under Long Duration Ground Motions." In *16th World Conference on Earthquake, 16WCEE 2017*, January 2017. Santiago, Chile: Chilean Association on Seismology and Earthquake Engineering (ACHISINA).

- He, W., J. Qiao, H. Xu, and J. Huang. 2023. "Experiment Investigation and Dynamic Responses of Three-Dimensional Isolation System with High-Static-Low-Dynamic Stiffness." *Soil Dynamics and Earthquake Engineering* 165 (February): 107679. <https://doi.org/10.1016/j.soildyn.2022.107679>.
- Hu, Z.-W., Z.-D. Xu, Y. Tian, Z.-H. Chen, J.-X. He, J. Dai, Q.-S. Miao, and X.-L. Du. 2024. "Test, Modeling, and Vibration Control of a Novel Viscoelastic Multi-Dimensional Earthquake Isolation and Mitigation Device." *Actuators* 13 (12): 481. <https://doi.org/10.3390/act13120481>.
- Inoue, K., M. Fushimi, S. Moro, M. Morishita, S. Kitamura, and T. Fujita. 2004. "Development of Three-Dimensional Seismic Isolation System for Next Generation Nuclear Power Plant." In *Proceedings of the 13th World Conference on Earthquake Engineering*, 1–6. Vancouver, BC: 13 WCEE Secretariat.
- Koo, G.-H., J. Jin-Young, J.-K. Hwang, T.-M. Shin, and L. Min-Seok. 2022. "Vertical Seismic Isolation Device for Three-Dimensional Seismic Isolation of Nuclear Power Plant Equipment—Case Study." *Applied Sciences* 12 (1): 320. <https://doi.org/10.3390/app12010320>.
- Kumar, M., A. S. Whittaker, and M. C. Constantinou. 2014. "An Advanced Numerical Model of Elastomeric Seismic Isolation Bearings." *Earthquake Engineering & Structural Dynamics* 43 (13): 1955–1974. <https://doi.org/10.1002/eqe.2431>.
- Kumar, S., and M. Kumar. 2021. "Damping Implementation Issues for In-Structure Response Estimation of Seismically Isolated Nuclear Structures." *Earthquake Engineering & Structural Dynamics* 50 (7): 1967–1988. <https://doi.org/10.1002/eqe.3436>.
- Liang, Q., W. Luo, Y. Zhou, X. Ke, and J. Li. 2022. "Seismic Performance of a Novel Three-Dimensional Isolation Bearing." *Journal of Building Engineering* 57 (October): 104818. <https://doi.org/10.1016/j.job.2022.104818>.
- Luo, W., Q. Liang, Y. Zhou, Z. Lu, J. Li, and Z. He. 2024. "A Novel Three-Dimensional Isolation Bearing for Buildings Subject to Metro- and Earthquake-Induced Vibrations: Laboratory Test and Application." *Journal of Building Engineering* 86 (June): 108798. <https://doi.org/10.1016/j.job.2024.108798>.
- Mazza, F., and R. Labernarda. 2017. "Structural and Non-Structural Intensity Measures for the Assessment of Base-Isolated Structures Subjected to Pulse-Like Near-Fault Earthquakes." *Soil Dynamics and Earthquake Engineering* 96 (May): 115–127. <https://doi.org/10.1016/j.soildyn.2017.02.013>.
- McKenna, F., M. H. Scott, and G. L. Fenves. 2000. "OpenSees, Open System for Earthquake Engineering Simulation." Moghaddam, H., I. Hajirasouliha, and A. Doostan. 2005. "Optimum Seismic Design of Concentrically Braced Steel Frames: Concepts and Design Procedures." *Journal of Constructional Steel Research* 61 (2): 151–166. <https://doi.org/10.1016/j.jcsr.2004.08.002>.
- Morishita, M., K. Inoue, and T. Fujita. 2004. "Development of Three-Dimensional Seismic Isolation Systems for Fast Reactor Application." *Journal of Japan Association for Earthquake Engineering* 4 (3): 305–310. https://doi.org/10.5610/jaee.4.3_305.
- Pant, D. R., A. C. Wijeyewickrema, and M. A. ElGawady. 2013. "Appropriate Viscous Damping for Nonlinear Time-History Analysis of Base-Isolated Reinforced Concrete Buildings." *Earthquake Engineering & Structural Dynamics* 42 (15): 2321–2339. <https://doi.org/10.1002/eqe.2328>.
- Pietra, D., and A. Park. 2016. "Behaviour and Modelling of Lead-Rubber Bearings Subjected to Tensile Actions." <https://www.semanticscholar.org/paper/BEHAVIOUR-AND-MODELLING-OF-LEAD-RUBBER-BEARINGS-TO-Pietra-Park/91e62ff2996ea3a1948feac248100c5cc980ee68>.
- Pourmasoud, M. M., J. B. P. Lim, I. Hajirasouliha, and D. McCrum. 2020. "Multi-Directional Base Isolation System for Coupled Horizontal and Vertical Seismic Excitations." *Journal of Earthquake Engineering* 26 (3): 1145–1170. January 1–26. <https://doi.org/10.1080/13632469.2020.1713925>.
- Ryan, K. L., S. Soroushian, E. Maragakis, E. Sato, T. Sasaki, and T. Okazaki. 2016. "Seismic Simulation of an Integrated Ceiling-Partition Wall-Piping System at E-Defense. I: Three-Dimensional Structural Response and Base Isolation." *Journal of Structural Engineering* 142 (2): 04015130. [https://doi.org/10.1061/\(ASCE\)ST.1943-541X.0001384](https://doi.org/10.1061/(ASCE)ST.1943-541X.0001384).
- Sarlis, A. A., D. T. R. Pasala, M. C. Constantinou, A. M. Reinhorn, S. Nagarajaiah, and D. P. Taylor. 2013. "Negative Stiffness Device for Seismic Protection of Structures." *Journal of Structural Engineering* 139 (7): 1124–1133. [https://doi.org/10.1061/\(ASCE\)ST.1943-541X.0000616](https://doi.org/10.1061/(ASCE)ST.1943-541X.0000616).
- Shi, Y., Y. Wang, M. Zhang, Y. Ding, and Z.-X. Li. 2023. "Seismic Performance Analysis of Steel Frame Structures with Separated Three-Dimensional Isolation." *Earthquake Engineering and Resilience* 2 (1): 52–73. <https://doi.org/10.1002/eer2.41>.
- Skinner, R. I., W. H. Robinson, and G. H. McVerry. 1993. *An Introduction to Seismic Isolation*. Chichester: Wiley.
- Soroushian, S., E. Maragakis, K. L. Ryan, E. Sato, T. Sasaki, T. Okazaki, and G. Mosqueda. 2016. "Seismic Simulation of an Integrated Ceiling-Partition Wall-Piping System at E-Defense. II: Evaluation of Nonstructural Damage and Fragilities." *Journal of Structural Engineering* 142 (2): 04015131. [https://doi.org/10.1061/\(ASCE\)ST.1943-541X.0001385](https://doi.org/10.1061/(ASCE)ST.1943-541X.0001385).
- Suhara, J., R. Matsumoto, S. Oguri, Y. Okada, K. Inoue, and K. Takahashi. 2005. "Research on 3-D Base Isolation System Applied to New Power Reactor 3-D Seismic Isolation Device with Rolling Seal Type Air Spring: Part 2." In *18th International Conference on Structural Mechanics in Reactor Technology (SMiRT 18)*, August 2005. Beijing, China: International Association for Structural Mechanics in Reactor Technology (IASMiRT).

- Vaiana, N., R. Capuano, S. Sessa, F. Marmo, and L. Rosati. 2021. "Nonlinear Dynamic Analysis of Seismically Base-Isolated Structures by a Novel OpenSees Hysteretic Material Model." *Applied Sciences* 11 (3): 900. <https://doi.org/10.3390/app11030900>.
- Vu, B., M. Unal, G. P. Warn, and A. M. Memari. 2014. "A Distributed Flexibility and Damping Strategy to Control Vertical Accelerations in Base-Isolated Buildings." *Structural Control & Health Monitoring* 21 (4): 503–521. <https://doi.org/10.1002/stc.1580>.
- Warn, G. P., and B. Vu. 2012. "Exploring the Low Shape Factor Concept to Achieve Three-Dimensional Seismic Isolation." In *20th Analysis and Computation Specialty Conference*, 1–11. Chicago, IL: American Society of Civil Engineers. <https://doi.org/10.1061/9780784412374.001>.
- Xu, H., W. He, L. Zhang, and W. Liu. 2023. "Shaking Table Test of a Novel Three-Dimensional Seismic Isolation System with Inclined Rubber Bearings." *Engineering Structures* 293 (October): 116609. <https://doi.org/10.1016/j.engstruct.2023.116609>.
- Yabana, S., and A. Matsuda. 2000. "Mechanical Properties of Laminated Rubber Bearings for Three-Dimensional Seismic Isolation." In *12th World Conference on Earthquake Engineering*, edited by T. Paulay. Auckland, New Zealand, Paper.
- Yu, T., C. Zhang, Z. Huang, W. Huang, S. Wang, G. Zhong, and D. Ou. 2023. "Experimental and Numerical Studies of a Novel Three-Dimensional Isolation Device Incorporating Disc Springs with U-Shaped Dampers." *Soil Dynamics and Earthquake Engineering* 174 (November): 108164. <https://doi.org/10.1016/j.soildyn.2023.108164>.
- Zhang, H., Q. Han, Y. Wang, and Y. Lu. 2016. "Explicit Modeling of Damping of a Single-Layer Latticed Dome with an Isolation System Subjected to Earthquake Ground Motions." *Engineering Structures* 106 (January): 154–165. <https://doi.org/10.1016/j.engstruct.2015.10.027>.
- Zhou, Z., J. Wong, and S. Mahin. 2016. "Potentiality of Using Vertical and Three-Dimensional Isolation Systems in Nuclear Structures." *Nuclear Engineering and Technology* 48 (5): 1237–1251. <https://doi.org/10.1016/j.net.2016.03.005>.